

## Compression of albite, NaAlSi<sub>3</sub>O<sub>8</sub>

MATTHEW D. BENUSA, ROSS J. ANGEL,\* AND NANCY L. ROSS

Crystallography Laboratory, Department of Geosciences, Virginia Polytechnic Institute and State University, Blacksburg, Virginia 24061, U.S.A.

### ABSTRACT

The structure and equation of state of low albite, NaAlSi<sub>3</sub>O<sub>8</sub>, has been determined using high-pressure single-crystal X-ray diffraction to a maximum pressure of 9.43 GPa. Low albite remains triclinic in space group  $C\bar{1}$  over the entire pressure range and no phase transitions were observed although the evolution of the unit-cell parameters and volume exhibit some unusual features at pressures above 4 GPa. A third-order Birch-Murnaghan equation of state fit to 6  $P$ - $V$  data points up to 3.4 GPa has  $K_0 = 54.2(7)$  GPa and  $K' = 5.3(6)$ . At higher pressures the volume-pressure curve exhibits  $d^2V/dP^2 < 0$  and the entire  $P$ - $V$  data set can be approximated with a fourth-order Birch-Murnaghan equation of state with  $K_0 = 52.3(9)$  GPa,  $K'_0 = 8.8(6)$ , and  $K''_0 = -2.8(2)$  GPa<sup>-1</sup>.

The anisotropy of the compression of albite is typical of that of feldspars with 65% of the volume compression accounted for by the compression of the (100) plane normal. This is due to the closing-up of the crankshaft chains of tetrahedra that are characteristic of the feldspar structure. Single-crystal X-ray intensity data sets collected at 6.4, 8.4, and 9.4 GPa also show that the four-membered rings of tetrahedra within the structure undergo significant shear at high pressures. Changes in the rate of shear of the four-membered rings with pressure are associated with changes in the variation of the unit-cell angles with pressure.

### INTRODUCTION

The feldspars comprise 60% of the volume of the Earth's crust. Although they are not thermodynamically stable at pressures in excess of 1 GPa in geological environments, compressional studies at higher pressures can provide more accurate equation of state (EoS) data for petrological applications. Recent determinations of the EoS of plagioclase feldspars (Angel 2004b) revealed some complexities in their response to pressure. While anorthite-rich plagioclase have EoS characterized by values of  $K' = \partial K/\partial P < 4$ , albite was previously reported to have  $K' > 4$  (Downs et al. 1994). The low-pressure EoS of An<sub>20</sub> plagioclase (Angel 2004b) resembles that of albite with  $K' > 4$ , but at pressures above 3.5 GPa the EoS of this plagioclase exhibits a turnover and  $K'$  becomes less than 4 and thus more typical of anorthite-rich plagioclase. As the previous EoS and structural data for albite was limited to a maximum pressure of 4 GPa (Downs et al. 1994), we undertook this study to significantly higher pressures so as to provide more precise EoS parameters and to determine whether it too exhibits a turnover in its EoS.

### EXPERIMENTAL METHODS

The sample used in this study is from the Amelia Court House locality in Virginia and was taken from the collection in the Geosciences Museum at Virginia Polytechnic Institute and State University. Amelia albite was chosen because it has been extensively characterized by previous workers. Carpenter et al. (1985) determined the composition to be Ab<sub>98</sub>Or<sub>1</sub>An<sub>1</sub>. It has an almost completely ordered aluminum/silicon distribution in a triclinic  $C\bar{1}$  structure (Carpenter et al. 1985; Harlow and Brown 1980; Kirkpatrick et al. 1985; Smith et al. 1986). The unit-cell parameters determined from this study at room pressure (Table 1) show good agreement with those previously reported in the literature for albite from this locality. A single crystal in the form of a plate of approximate dimensions 110

× 120 × 28 μm was loaded in an ETH-designed diamond-anvil cell (Miletich et al. 2000) with a T301 steel gasket indented to 60 μm thickness and drilled out to 250 μm diameter. A ruby chip was added for approximate pressure measurement and a quartz crystal was used as an internal diffraction pressure standard. A 4:1 mixture of methanol and ethanol was used as the pressure-transmitting medium. The constant widths of ~0.05° of the rocking curves for the diffraction peaks of quartz at all pressures indicated that the pressure medium remained hydrostatic up to the highest pressure achieved, 9.43(2) GPa. The unit-cell parameters of the albite were determined at each pressure from a least-squares fit to the corrected setting angles of 20–22 reflections in the 2θ range of 10.8° to 25.5° obtained by the eight-position centering method (King and Finger 1979) with a Huber four-circle diffractometer using unfiltered MoKα radiation (λ = 0.7107 Å). Full details of the instrument and the peak-centering algorithms are provided by Angel et al. (1997, 2000). Pressures were determined from the unit-cell volumes of the quartz crystal in the diamond anvil cell, using the equation of state reported by Angel et al. (1997). Equation of state parameters for albite were obtained by a weighted least-squares fit (Angel 2000) of the Birch-Murnaghan equation of state (Birch 1947) to the pressure-volume data. The unit-cell parameters and volume of albite as a function of pressure measured in this study are reported in Table 1.

The structure of albite was previously determined at 5 pressures up to a maximum of 3.8 GPa by Downs et al. (1994). We therefore only collected intensity data at higher pressures (6.49, 8.41, and 9.43 GPa) with an Xcalibur-1 diffractometer equipped with monochromated MoKα radiation and both point and CCD detectors. At 8.41 and 9.43 GPa initial data collections were performed with the CCD detector to verify that no additional reflections indicative of symmetry changes had appeared in the diffraction patterns. Intensity data sets for structure refinement were collected with the point detector. The resulting step-scan data were integrated with the WinIntegrStp program (Angel 2003), data reduction was performed with the Absorb program (Angel 2004a), and structure refinements with RFINE (Finger and Prince 1974). Following Downs et al. (1994) we refined all of the atom positions independently without restraints or constraints with isotropic displacement parameters for the framework atoms but anisotropic displacement parameters to account for the substantial anisotropy of the Na atom. Refined positional parameters are reported in Table 2 and selected bond lengths and angles in Tables 3 and 4.

### RESULTS

Albite remained triclinic in space group  $C\bar{1}$  to the highest pressure attained. From room pressure up to the maximum pres-

\* E-mail: rangel@vt.edu

**TABLE 1.** Unit-cell parameters of albite measured in this study

Pressure GPa	<i>a</i> (Å)	<i>b</i> (Å)	<i>c</i> (Å)	$\alpha$ (°)	$\beta$ (°)	$\gamma$ (°)	<i>V</i> (Å <sup>3</sup> )
0.001(0)	8.1409(8)	12.7883(5)	7.1602(7)	94.251(7)	116.586(7)	87.676(6)	664.760(85)
0.455(7)	8.1074(10)	12.7678(5)	7.1481(6)	94.246(9)	116.683(8)	87.717(7)	659.272(90)
1.438(7)	8.0381(12)	12.7280(5)	7.1231(7)	94.246(8)	116.839(10)	87.794(7)	648.46(10)
2.145(8)	7.9919(9)	12.7004(5)	7.1064(6)	94.234(9)	116.928(8)	87.849(7)	641.320(79)
2.358(8)	7.9773(7)	12.6929(4)	7.1004(7)	94.220(7)	116.945(6)	87.868(6)	639.184(76)
3.365(9)	7.9142(8)	12.6575(4)	7.0794(7)	94.188(8)	117.045(8)	87.951(6)	629.937(78)
4.323(8)	7.8542(9)	12.6256(5)	7.0572(7)	94.138(9)	117.099(8)	88.022(7)	621.387(87)
5.227(9)	7.7974(7)	12.5964(5)	7.0388(6)	94.070(8)	117.143(7)	88.089(6)	613.655(71)
5.859(11)	7.7580(7)	12.5772(4)	7.0251(5)	94.021(7)	117.156(7)	88.116(5)	608.411(68)
6.489(11)	7.7176(6)	12.5592(4)	7.0113(4)	93.963(6)	117.177(6)	88.132(5)	603.114(60)
6.930(12)	7.6863(8)	12.5473(4)	7.0048(7)	93.908(7)	117.228(8)	88.111(5)	599.237(78)
7.252(12)	7.6646(5)	12.5399(3)	6.9957(4)	93.877(6)	117.223(5)	88.072(4)	596.525(55)
7.702(11)	7.6306(4)	12.5303(2)	6.9861(3)	93.831(4)	117.268(4)	87.963(3)	592.406(41)
7.897(12)	7.6150(6)	12.5258(3)	6.9813(5)	93.826(6)	117.298(6)	87.877(4)	590.408(60)
8.411(11)	7.5713(5)	12.5170(3)	6.9697(5)	93.797(5)	117.448(5)	87.508(4)	584.809(54)
8.939(13)	7.5339(7)	12.5053(3)	6.9575(6)	93.830(6)	117.630(7)	87.104(5)	579.302(67)
9.181(15)	7.5190(4)	12.4991(2)	6.9517(6)	93.852(4)	117.711(5)	86.942(3)	576.901(55)
9.431(15)	7.5028(7)	12.4933(4)	6.9463(6)	93.903(7)	117.791(6)	86.786(5)	574.459(63)

Note: The figures in parentheses represent 1 e.s.d. of the last decimal place shown.

**TABLE 2.** Refined parameters for albite

Pressure (GPa)	Atom	<i>x</i>	<i>y</i>	<i>z</i>	<i>B<sub>eq</sub>/B<sub>iso</sub></i> *	
6.489(11)	Na	0.2490(9)	0.9935(3)	0.1490(16)	2.5(5)	
	T1o	-0.0021(6)	0.16648(16)	0.2025(11)	0.69(4)	
	T1m	-0.0096(6)	0.82031(15)	0.2349(11)	0.58(4)	
	T2o	0.6867(8)	0.10437(16)	0.3121(13)	0.44(4)	
	T2m	0.6558(8)	0.87698(15)	0.3551(14)	0.50(4)	
	Oa1	0.0115(14)	0.1286(4)	0.968(3)	0.98(9)	
	Oa2	0.5675(14)	0.9956(4)	0.284(3)	0.60(8)	
	Obo	0.7989(14)	0.0923(4)	0.168(3)	0.86(9)	
	Obm	0.7872(15)	0.8436(4)	0.237(3)	1.10(9)	
	Oco	-0.0285(14)	0.2993(4)	0.265(3)	0.78(9)	
	Ocm	0.0150(15)	0.6929(4)	0.223(3)	1.13(9)	
	Odo	0.2184(19)	0.1171(5)	0.396(4)	1.35(13)	
	Odm	0.1618(19)	0.8737(5)	0.431(4)	1.68(13)	
	8.411(11)	Na	0.2414(8)	0.9923(3)	0.1587(14)	2.1(5)
		T1o	-0.0096(6)	0.16881(14)	0.2005(10)	0.53(3)
		T1m	-0.0191(6)	0.82206(12)	0.2318(9)	0.48(3)
		T2o	0.6867(7)	0.10187(13)	0.3131(11)	0.43(3)
T2m		0.6460(7)	0.87521(13)	0.3516(12)	0.47(3)	
Oa1		0.0133(13)	0.1306(4)	0.970(3)	1.03(8)	
Oa2		0.5645(13)	0.9966(4)	0.294(2)	0.57(7)	
Obo		0.7919(13)	0.0899(4)	0.160(3)	0.89(8)	
Obm		0.7641(13)	0.8398(4)	0.213(3)	0.95(8)	
Oco		-0.0446(12)	0.3014(4)	0.265(3)	0.65(7)	
Ocm		0.0294(13)	0.6970(4)	0.254(3)	0.97(8)	
Odo		0.2117(17)	0.1233(4)	0.395(3)	1.33(10)	
Odm		0.1445(17)	0.8857(4)	0.436(3)	1.61(10)	
9.431(15)		Na	0.2367(7)	0.9905(2)	0.1659(13)	1.1(4)
		T1o	-0.0159(5)	0.17068(14)	0.1989(10)	0.58(3)
		T1m	-0.0233(5)	0.82420(12)	0.2310(9)	0.50(3)
		T2o	0.6907(5)	0.10098(12)	0.3197(10)	0.49(3)
	T2m	0.6399(6)	0.87498(12)	0.3462(10)	0.45(3)	
	Oa1	0.0136(12)	0.1329(4)	0.969(3)	0.93(8)	
	Oa2	0.5569(11)	0.9985(3)	0.2912(19)	0.60(7)	
	Obo	0.7858(12)	0.0904(4)	0.155(3)	0.86(8)	
	Obm	0.7530(11)	0.8395(4)	0.202(2)	0.92(7)	
	Oco	-0.0550(10)	0.3039(3)	0.2624(19)	0.69(8)	
	Ocm	0.0370(11)	0.7006(4)	0.271(3)	0.92(8)	
	Odo	0.2103(14)	0.1278(4)	0.397(3)	1.09(9)	
	Odm	0.1306(12)	0.8953(4)	0.434(3)	1.15(8)	

\* All atoms except for Na were refined with isotropic displacement parameters.

pressure attained the volume of albite decreased by 13.6% (Fig. 1). The new volume-pressure data is in excellent agreement with that previously reported by Downs et al. (1994) up to 3.8 GPa. A fit of our 6 data points up to 3.4 GPa yielded bulk modulus values of  $K_0 = 54.2(7)$  GPa and  $K' = 5.3(6)$  for a third-order Birch-Murnaghan EoS. These values are indistinguishable from those reported by

**TABLE 3.** Tetrahedral bond lengths in albite (Å)

		6.49 GPa	8.41 GPa	9.43 GPa
T1o	Oa1	1.729(12)	1.730(12)	1.744(12)
T1o	Obo	1.735(7)	1.736(6)	1.737(5)
T1o	Oco	1.726(6)	1.732(5)	1.737(5)
T1o	Odo	1.748(18)	1.702(16)	1.698(14)
Average		1.735	1.725	1.729
T1m	Oa1	1.593(12)	1.580(11)	1.555(13)
T1m	Obm	1.594(6)	1.593(6)	1.596(5)
T1m	Ocm	1.606(5)	1.593(5)	1.590(6)
T1m	Odm	1.53(2)	1.583(17)	1.593(12)
Average		1.582	1.587	1.584
T2o	Oa2	1.622(6)	1.605(5)	1.616(5)
T2o	Obo	1.600(9)	1.596(8)	1.599(9)
T2o	Ocm	1.620(9)	1.580(7)	1.589(6)
T2o	Odm	1.650(18)	1.622(16)	1.607(14)
Average		1.623	1.601	1.603
T2m	Oa2	1.630(7)	1.620(6)	1.632(6)
T2m	Obm	1.604(9)	1.623(8)	1.617(8)
T2m	Oco	1.600(10)	1.593(8)	1.596(6)
T2m	Odo	1.563(19)	1.587(16)	1.605(16)
Average		1.599	1.606	1.613

**TABLE 4.** T-O-T bond angles (°) in albite as a function of pressure

		6.49 GPa	8.41 GPa	9.43 GPa
T1o	Oa1	T1m	140.2(4)	141.9(3)
T2m	Oa2	T2o	127.8(6)	128.9(5)
T2o	Obo	T1o	126.4(8)	122.3(7)
T2m	Obm	T1m	153.0(12)	143.1(10)
T1o	Oco	T2m	119.4(4)	115.7(3)
T1m	Ocm	T2o	138.9(8)	149.3(5)
T1o	Odo	T2m	139.1(6)	144.2(6)
T1m	Odm	T2o	156.0(6)	153.8(5)

Downs et al. (1994) for data collected to 3.8 GPa.

However, at pressures in excess of 4 GPa the volume-pressure data fall significantly beneath the extrapolation of the lower-pressure EoS (Fig. 1) indicating that the structure has become elastically softer than at lower pressures. This unusual behavior is also apparent in an  $f$ - $F$  (normalized stress-finite strain) plot derived from the measured volume-pressure data. For the Birch-Murnaghan EoS the finite strain is  $f_E = [(V_0/V)^{2/3} - 1]/2$ , the normalized stress is defined as  $F_E = P/3f_E^2$ , and the EoS can be rewritten as a polynomial in the strain (Stacey et al. 1981):

$$F_E = K_0 + (3K_0/2)(K_0 - 4)f_E + (3K_0/2)[(K_0K'' + (K' - 4)K' - 3) + (35/9)]f_E^2 + \dots$$

While the initial slope of the  $f$ - $F$  plot (Fig. 2) is positive, which confirms that  $K'_0$  is greater than 4, the slope decreases until at 3.9 GPa it becomes zero before becoming negative at higher pressures. This is similar to the behavior previously reported for albite-rich plagioclase (Angel 2004b). This curvature requires that at least a fourth-order EoS be used to fit the entire data set, yielding  $K_0 = 52.3(9)$  GPa,  $K'_0 = 8.8(6)$ , and  $K''_0 = -2.8(2)$  GPa<sup>-1</sup>. However, it is not clear that the Birch-Murnaghan EoS has any validity with such parameter values beyond that of representing

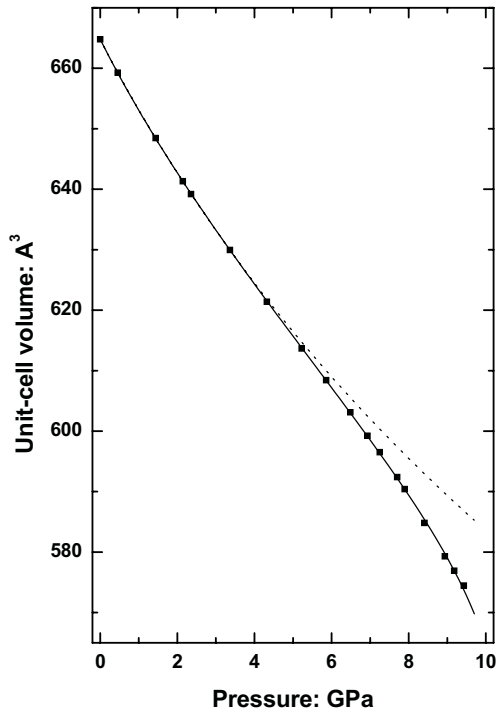


**FIGURE 1.** The pressure-volume data measured for albite in this study. The broken line is the third-order Birch Murnaghan EoS fitted to data below 3.5 GPa. The measured data deviate from the extrapolation of the third-order EoS above 5 GPa and can only be approximately represented by a fourth-order Birch-Murnaghan EoS, as shown as the solid line.

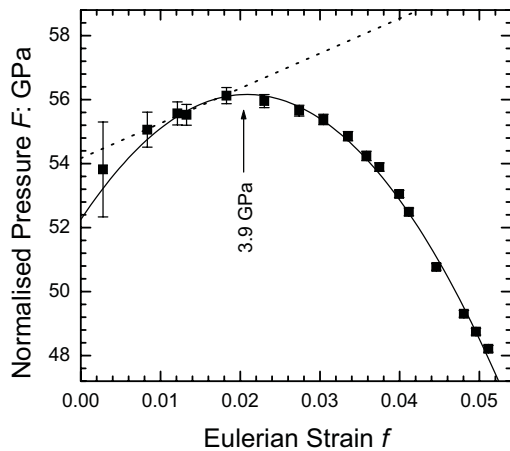


**FIGURE 2.** The pressure-volume data plotted as the normalized stress,  $F$ , against the Eulerian strain,  $f$ . The broken line is the third-order Birch Murnaghan EoS fitted to data below 3.5 GPa. Error bars include experimental uncertainties in volume, pressure, and  $V_0$  (Angel 2000).

the data. Nonetheless, it does show that above 4.9 GPa the bulk modulus of albite starts to decrease from a peak value of ~73 GPa and that  $K'$  becomes negative (Fig. 3). At pressures above 8.4 GPa albite is softer than at room pressure. The same softening is apparent in the  $P$ - $V$  plot (Fig. 1) that clearly exhibits a downward curvature, or  $d^2V/dP^2 < 0$ , above 4.9 GPa.

Calculation of the strain tensor (Ohashi and Burnham 1973) from the unit-cell parameters shows that the compression of albite is very anisotropic, with 65% of the total compression over the entire pressure range being accommodated along a direction close to the (100) plane normal. This is typical of the behavior of all feldspars that have been studied (e.g., Angel 1994, 2004b; Downs et al. 1994). Closer inspection of the variation of the unit-cell parameters with pressure indicates that both the (100) plane normal and  $\mathbf{a}$  appear to become softer with increasing pressure (Fig. 4). The  $b$  and  $c$  unit-cell parameters show normal compressional behavior up to 5 GPa, but at higher pressures there is an increase in the rate of stiffening in  $\mathbf{b}$  and a softening of  $\mathbf{c}$ . Furthermore, at pressures above 8 GPa the minor axis of the strain ellipsoid closest to the [110] direction becomes marginally positive. That is, at pressures in excess of 8 GPa the application of hydrostatic pressure results in an expansion, rather than a contraction, of the [110] direction (Fig. 4). This expansion is due to the rapid decrease in the  $\gamma$  unit-cell angle at pressures in excess of 6.5 GPa (Fig. 5).

The reasons for the complex behavior of the unit-cell parameters lie in the response of the tetrahedral framework to pressure. The average bond lengths of the four tetrahedra over the entire pressure range (Table 3) show only very small changes. The major changes in the albite structure upon compression can

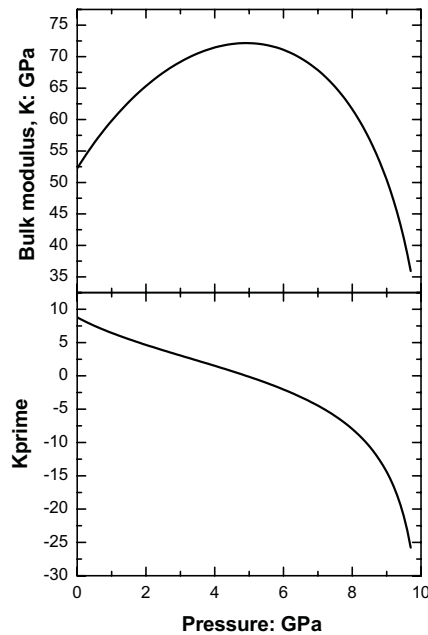


**FIGURE 3.** The variation with pressure of the bulk modulus,  $K$ , and its pressure derivative  $K'$ , derived from the fourth-order Birch-Murnaghan EoS fitted to the  $P$ - $V$  data. The decrease in bulk modulus at pressures above 5 GPa reflects the downward curvature seen in the  $P$ - $V$  data shown in Figure 1.

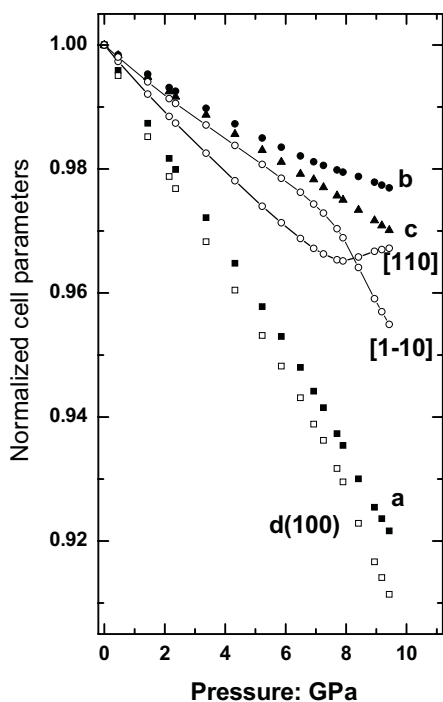


FIGURE 4. The variation of the unit-cell parameters and other directions in albite as a function of pressure, normalized to their room pressure values. The maximum compression in the structure remains approximately parallel to the (100) plane normal over the entire pressure range. Note that above 5 GPa the *b* cell edge becomes stiffer and the  $[1\bar{1}0]$  direction becomes softer than at lower pressures. At 8 GPa the  $[110]$  direction starts to expand. Symbol sizes exceed the estimated standard uncertainties in the measurements.

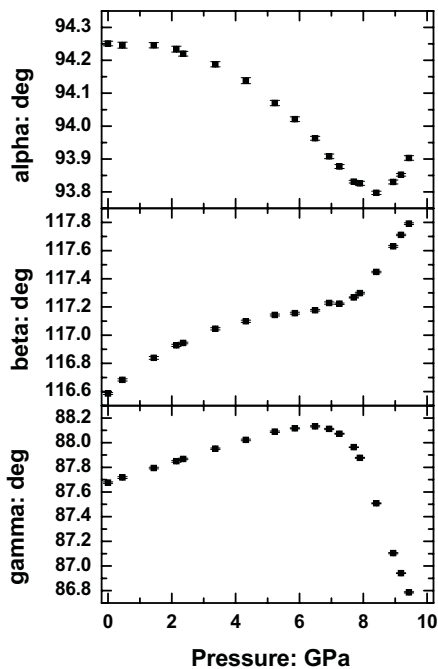


FIGURE 5. The variation of the unit-cell angles of albite with pressure. The changes in the trends at 5, 7, and 8.5 GPa appear to be correlated with changes in the compression of the T-O-T bond angles within the structure. Error bars indicate one estimated standard uncertainty.

therefore be described as being due to the flexing of an essentially rigid tetrahedral framework as reflected in changes in the T-O-T bond angles (Table 4 and Fig. 6). The refined structure at 6.49 GPa mostly reflects a simple extension of the trends identified by Downs et al. (1994) in their study of albite up to 3.8 GPa. The biggest structural changes are the reduction in the T-Obo-T and T-Oco-T bond angles (Fig. 6) which result in the closing-up of the crankshaft chains that run parallel to  $[100]$  in the structure. The T1o-T2o-T1m-T2m four-membered rings of tetrahedra (labeled “Ring 1” in Fig. 7) also undergo significant shear as indicated by the changes in the O-O-O angles around this ring (Fig. 8).

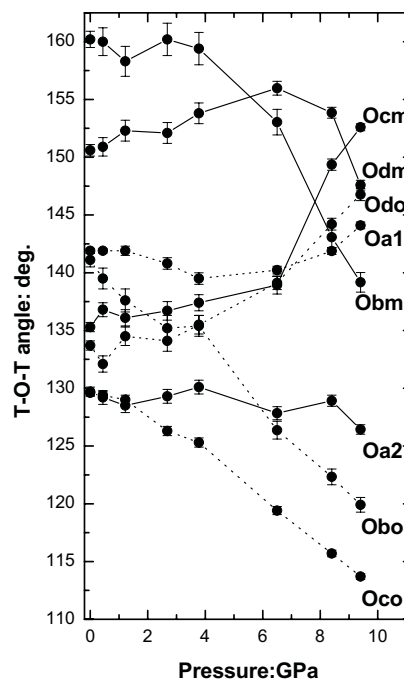


FIGURE 6. The variation of the T-O-T angles in albite with pressure. The lines are drawn as guides to the eye, with broken lines indicating oxygen atoms bonded to the Al-containing T1o site. Data below 4 GPa is taken from Downs et al. (1994), data above 4 GPa is from this work.

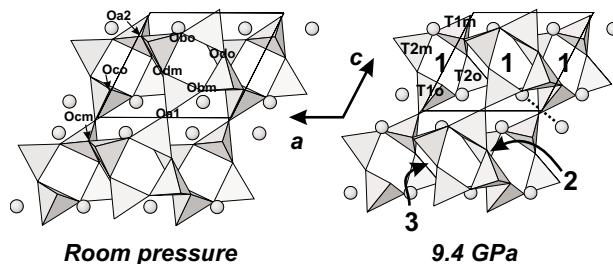
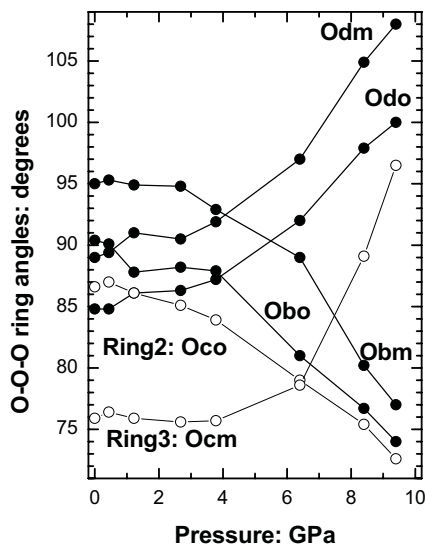


FIGURE 7. Polyhedral representations of the structure of albite at room pressure (from Downs et al. 1994) and at 9.43 GPa (this work) projected down the  $[010]$  axis. The drawing is limited to atoms lying between  $y = 0$  and  $y = \frac{1}{2}$ . The large numerals on the right-hand diagram identify the three distinct four-membered rings of tetrahedra that form the crankshaft chains that run parallel to *a*. The pressure-induced shear of ring 1 is very obvious in this view. The dashed line indicates the shortest Na-Na distance in the structure that forms part of the Oa2-Na-Na-Oa2 strut discussed by Megaw (1970).

The resulting narrowing of the channels bridged by these rings is responsible for the softness of the (100) plane normal that is typical of the compression of all feldspars (e.g., Allan and Angel 1997; Downs et al. 1994, 1999).

The other changes in the compression of the structure that give rise to the softening and to the changes in bond-angle trends at higher pressures are overlain upon the primary trend of closing-up of the crankshafts. The maximum in the bulk modulus at 4.9 GPa (Fig. 3) would appear to be related to the initiation of significant tilting of both T1 tetrahedra around the [001] direction at some pressure between 3.8 and 6.49 GPa. This tilting gives rise to an increase in the rate of change of the T1m-Obm-T2m angle (Fig. 6), an increased rate of shear of the T1o-T2o-T1m-T2m ring (ring 1 in Fig. 7) as measured by O-O-O angles (Fig. 8), and the initiation of significant shear of the other two four-membered rings that form the sides of the crankshaft chains (Fig. 8). This change in compression pattern, the saturation in the variation of the  $\beta$  unit-cell angle with pressure between 6 and 8 GPa (Fig. 5), and subsequent increase is similar to that observed for microcline (Allan and Angel 1997). In microcline this was attributed to the formation of a new bond between the K atom and the Obm atom in the framework as the framework is compressed (Downs et al. 1999). In contrast to microcline, we find that in albite the Na-Obm distance remains greater than 3 Å at all pressures, and pro-molecule calculations of the electron density based on the refined structure at 9.43 GPa clearly show that it remains a non-bonded contact. The change in the variation of the  $\beta$  unit-cell angle in albite between 6 and 8 GPa is associated with a change in the rate of increase of the T-Ocm-T and T-Odo-T angles with pressure (Fig. 6), and the resulting increase in the rate of shear of the four-membered rings of tetrahedra we have called Ring 1 and Ring 3 (Fig. 8). The inversion in the trend of the  $\alpha$  unit-cell



**FIGURE 8.** The shear of the four-membered rings of tetrahedra in albite as measured by the O-O-O angles. The solid symbols are the four corners of the ring Obo-Odo-Obm-Odm (ring 1 as defined in Fig. 7), and the open symbols are one corner each of rings 2 and 3. Symmetry requires that the O-O-O angles in rings 2 and 3 occur as pairs, with the pairs being complementary angles. The data below 4 GPa is taken from Downs et al. (1994), data above 4 GPa is from this work.

angle at about 8.5 GPa (Fig. 5) is associated with the reversal of the trend of the T-Odm-T angle which, after a slight increase from room pressure to 8.4 GPa, decreases by 5° over the next 1 GPa (Fig. 6).

The shortest Na-Na distance, once proposed as part of the “Oa2-Na-Na-Oa2 strut” that was believed to force the crankshaft chains to open out (Megaw 1970), decreases linearly with pressure, as does the Na-Oa2 distance (Fig. 9). The pro-molecule calculations also show that the longer Na-Oco and Na-Odm contacts remain non-bonded at all pressures despite the significant decrease in the distances (Fig. 9). There are also significant decreases in both the anisotropy and the magnitude of the displacement parameters of the Na atom at pressure. It therefore seems reasonable to conclude that the Na atom plays a completely passive role in the compression of the structure, and that the large changes in Na-O distances with pressure are merely the result of the framework response to pressure, as suggested by Downs et al. (1994).

### CONCLUDING DISCUSSION

Over petrologically relevant ranges of pressure, the equation of state of albite reported by Downs et al. (1994) has been confirmed, with  $K' > 4$ . At higher pressures the closing-up of the crankshaft chains within the structure continues to be the dominant mechanism of compression and is responsible for the extreme anisotropy of compression that is typical for all feldspars (e.g., Angel 2004b; Angel et al. 1988) as well as the related framework of coesite (Angel et al. 2001). Changes in secondary mechanisms of compression in albite give rise to more complex behavior than has been previously observed in feldspars. At pressures above 4–5 GPa there is significant rotation of the T1 tetrahedra similar to that observed in coesite from room pressure (Angel et al. 2003). But in contrast to coesite, the initiation of this rotation in albite leads to softening of the

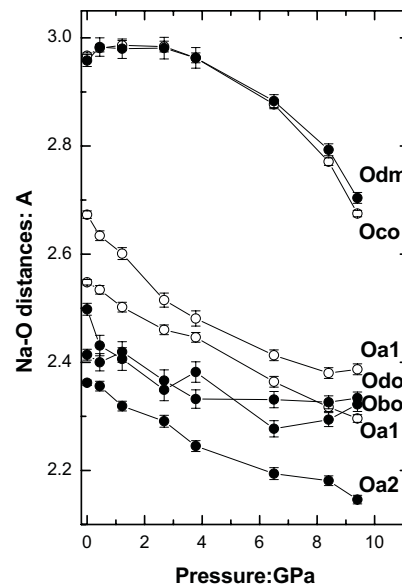


**FIGURE 9.** The variation of the Na-O distances in albite with pressure. The lines are drawn as guides to the eye. The data below 4 GPa is taken from Downs et al. (1994), data above 4 GPa is from this work.

structure and the turnover in the  $f$ - $F$  plot of the equation of state in albite. The same turnover in the EoS from a regime in which  $K' > 4$ , typical of alkali feldspars and albite at low pressures, to one in which  $K' < 4$ , typical of plagioclases with An contents higher than 30%, has been previously observed in albite-rich plagioclase feldspars (Angel 2004b). This suggests that there are two secondary compression mechanisms in feldspars, and both appear in albite at different pressures. At low pressures, albite exhibits compression of the crankshaft chains without rotation of the T1 tetrahedra and the associated shear of the tetrahedral four-membered rings (Downs et al. 1994). At higher pressures we may speculate on the basis of the similarities between their EoS that the plagioclase feldspars behave structurally in the same way as albite and that the rotation of the T1 tetrahedra we have observed in albite is typical of plagioclase compression at lower pressures.

A further change in behavior above 8 GPa involves severe softening of the structure as a whole (Fig. 3) while at the same time some directions in the structure start to expand as the pressure is increased. At these pressures the smallest T-O-T angle is reduced to less than  $115^\circ$  (Table 4), which is often considered an extreme limit for Al-O-Si or Si-O-Si bonds because it corresponds to an Al-Si distance of  $\sim 2.8 \text{ \AA}$ . All of these data therefore point to there being an elastic instability in albite at pressures slightly in excess of those achieved in this experiment that will result either in a phase transition to another crystalline phase or in pressure-induced amorphization similar to that found in anorthite and quartz (Daniel et al. 1997; Hazen et al. 1989).

#### ACKNOWLEDGMENTS

This work was supported by NSF grants EAR-0105864 and EAR-0408460. R.M. Hazen, A. Pawley, and an anonymous reviewer are thanked for their comments on an earlier version of this manuscript.

#### REFERENCES CITED

- Allan, D.R. and Angel, R.J. (1997) A high-pressure structural study of microcline ( $\text{KAlSi}_3\text{O}_8$ ) to 7 GPa. *European Journal of Mineralogy*, 9, 263–275.
- Angel, R. (2000) Equations of state. In R.M. Hazen and R.T. Downs, Eds., *High-Pressure and High-Temperature Crystal Chemistry. Reviews in Mineralogy*, 41, 35–60. Mineralogical Society of America, Washington, D.C.
- Angel, R.J. (1994) Feldspars at high pressure. In I. Parsons, Ed., *Feldspars and their Reactions*, C421, 271–312. Kluwer Academic Publishers, Dordrecht.
- (2003) Automated profile analysis for single-crystal diffraction data. *Journal of Applied Crystallography*, 36, 295–300.
- (2004a) Absorption corrections for diamond-anvil pressure cells implemented in a software package Absorb-6.0. *Journal of Applied Crystallography*, 37, 486–492.
- (2004b) Equations of state of plagioclase feldspars. *Contributions to Mineralogy and Petrology*, 146, 506–512.
- Angel, R.J., Hazen, R.M., McCormick, T.C., Prewitt, C.T., and Smyth, J.R. (1988) Comparative compressibility of end-member feldspars. *Physics and Chemistry of Minerals*, 15, 313–318.
- Angel, R.J., Allan, D.R., Miletich, R., and Finger, L.W. (1997) The use of quartz as an internal pressure standard in high-pressure crystallography. *Journal of Applied Crystallography*, 30, 461–466.
- Angel, R.J., Downs, R.T., and Finger, L.W. (2000) High-pressure, high-temperature diffraction. In R.M. Hazen and R.T. Downs, Eds., *High-Pressure and High-Temperature Crystal Chemistry. Reviews in Mineralogy*, 41, 559–596. Mineralogical Society of America, Washington, D.C.
- Angel, R.J., Mosenfelder, J.L., and Shaw, C.S.J. (2001) Anomalous compression and equation of state of coesite. *Physics of the Earth and Planetary Interiors*, 124, 71–79.
- Angel, R.J., Shaw, C.S.J., and Gibbs, G.V. (2003) Compression mechanisms of coesite. *Physics and Chemistry of Minerals*, 30, 167–176.
- Birch, F. (1947) Finite elastic strain of cubic crystals. *Physical Review*, 71, 809–824.
- Carpenter, M.A., McConnell, J.D.C., and Navrotsky, A. (1985) Enthalpies of ordering in the plagioclase feldspar solid solution. *Geochimica et Cosmochimica Acta*, 49, 947–966.
- Daniel, I., Gillet, P., McMillan, P.F., Wolf, G., and Verhelst, M.A. (1997) High-pressure behavior of anorthite: Compression and amorphization. *Journal of Geophysical Research, Solid Earth*, 102, 10313–10325.
- Downs, R., Hazen, R.M., and Finger, L.W. (1994) The high-pressure crystal chemistry of low albite and the origin of the pressure dependency of Al-Si ordering. *American Mineralogist*, 79, 1042–1052.
- Downs, R.T., Yang, H.X., Hazen, R.M., Finger, L.W., and Prewitt, C.T. (1999) Compressibility mechanisms of alkali feldspars: new data from reedmergerite. *American Mineralogist*, 84, 333–340.
- Finger, L. and Prince, E. (1974) A system of Fortran-IV computer programs for crystal structure computations. NBS technical note 854. National Bureau of Standards, Gaithersburg, MD, U.S.A.
- Harlow, G.E. and Brown, G.E. (1980) Low albite: an X-ray and neutron diffraction study. *American Mineralogist*, 65, 665–675.
- Hazen, R.M., Finger, L.W., Hemley, R., and Mao, H. (1989) High-pressure crystal chemistry and amorphisation of alpha-quartz. *Solid State Communications*, 72, 507–511.
- King, H. and Finger, L.W. (1979) Diffracted beam crystal centering and its application to high-pressure crystallography. *Journal of Applied Crystallography*, 12, 374–378.
- Kirkpatrick, R.J., Kinsey, R.A., Smith, K.A., Henderson, D.M., and Oldfield, E. (1985) High resolution solid-state sodium-23, aluminium-27, and silicon-29 nuclear magnetic resonance spectroscopic reconnaissance of alkali and plagioclase feldspar. *American Mineralogist*, 70, 106–123.
- Megaw, H. (1970) Structural relationship between coesite and feldspar. *Acta Crystallographica*, B26, 261–265.
- Miletich, R., Allan, D.R., and Kuhs, W.F. (2000) High-pressure single-crystal techniques. In R.M. Hazen and R.T. Downs, Eds., *High-Pressure and High-Temperature Crystal Chemistry. Reviews in Mineralogy*, 41, 445–519. Mineralogical Society of America, Washington, D.C.
- Ohashi, Y. and Burnham, C.W. (1973) Clinopyroxene lattice deformations: The roles of chemical substitution and temperature. *American Mineralogist*, 58, 843–849.
- Smith, J.V., Artioli, G., and Kvick, A. (1986) Low albite,  $\text{NaAlSi}_3\text{O}_8$ : Neutron diffraction study of crystal structure at 13K. *American Mineralogist*, 71, 727–733.
- Stacey, F., Brennan, B., and RD, I. (1981) Finite strain theories and comparisons with seismological data. *Geophysical Surveys*, 4, 189–232.

MANUSCRIPT RECEIVED SEPTEMBER 3, 2004

MANUSCRIPT ACCEPTED DECEMBER 22, 2004

MANUSCRIPT HANDLED BY ALISON PAWLEY